nature chemistry

ARTICLES

https://doi.org/10.1038/s41557-019-0353-3

Photoredox catalysis with aryl sulfonium salts enables site-selective late-stage fluorination

Jiakun Li[1], Junting Chen[1], Ruocheng Sang[1], Won-Seok Ham[1], Matthew B. Plutschack[1], Florian Berger[1], Sonia Chabbra[2], Alexander Schnegg[2], Christophe Genicot[3] and Tobias Ritter[1]*

Photoredox catalysis, especially in combination with transition metal catalysis, can produce redox states of transition metal catalysts to facilitate challenging bond formations that are not readily accessible in conventional redox catalysis. For arene functionalization, metallophotoredox catalysis has successfully made use of the same leaving groups as those valuable in conventional cross-coupling catalysis, such as bromide. Yet the redox potentials of common photoredox catalysts are not sufficient to reduce most aryl bromides, so synthetically useful aryl radicals are often not directly available. Therefore, the development of a distinct leaving group more appropriately matched in redox potential could enable new reactivity manifolds for metallophotoredox catalysis, especially if arylcopper(III) complexes are accessible, from which the most challenging bond-forming reactions can occur. Here we show the conceptual advantages of aryl thianthrenium salts for metallophotoredox catalysis, and their utility in site-selective late-stage aromatic fluorination.

Aryl fluorides are prevalent in active pharmaceuticals and agrochemicals; yet, late-stage site-selective C–F bond formation still remains a challenge. Metallophotoredox catalysis is useful because photoexcited catalysts can produce redox states of transition metal catalysts that can facilitate challenging bond formations, but that are not readily accessible in conventional redox catalysis[1–4]. The combination of photoredox catalysis with nickel provides access to both Ni(0) and Ni(III) species in the same catalytic cycle[5–7], which allows for both a fast oxidative addition of aryl electrophiles to Ni(0) and a fast product-forming reductive elimination from Ni(III) (refs [8–10]) (Fig. 1a). For carbon–fluorine reductive elimination, special ligands are required on nickel that have thus far not participated successfully in metallophotoredox catalysis, which illustrates the fundamental challenge of C–F bond formation[11]. Copper complexes are attractive catalysts because reductive elimination from Cu(III) can be more effective than that from Ni(III) (refs [12,13]). However, the oxidative addition to Cu(I) is slow, which has slowed down the development of copper-catalysed metallophotoredox catalysis. Aryl radicals can undergo oxidative ligation to copper, but the generation of aryl radicals from aryl halides has remained challenging[3]. One successful approach is atom abstraction with silyl radicals, which led to the trifluoromethylation of aryl bromides[14], but necessitates the use of an electrophile as the cross-coupling partner and the compatibility of the silyl reagents with the electrophile. The direct reduction of aryl halides to give aryl radicals and halide anions can be achieved and requires low reduction potentials[15–17], which can be reached with particularly reducing photocatalysts; the low reduction potential puts additional constraints on generating high-valent copper species in the same reaction medium. So far, C–F bond reductive elimination has not been reported for metallophotoredox-catalysed reactions. Here we report an approach to generate aryl radicals in the presence of high-valent copper species. We present the fundamental physical organic distinctions of aryl thianthrenium (ArTT) salts for metallophotoredox catalysis when compared to conventional aryl halides, and how they enable highly selective late-stage aromatic fluorination.

A general platform for photoredox–Cu(III) cross-coupling reactions should be enabled by suitable kinetic and thermodynamic reaction parameters for the reductive fragmentation of aryl (pseudo)halides. The standard reduction potentials of aryl halides and the rate constants for fragmentation of the corresponding aryl halide radical anions can be presented as a linear free-energy relationship (Fig. 1b). Electron-rich aryl halides are often prohibitively difficult to reduce, yet the corresponding putative aryl halide radical anions fragment rapidly, whereas the opposite is true for electron-poor aryl halides[18]. Efficient copper(III) photoredox cross-coupling requires both a suitable reduction potential of the aryl (pseudo) halide, positive enough to be accessible by a photoredox catalyst, and a sufficiently high fragmentation rate of the aryl halide radical anion to minimize undesired electron-transfer processes between the aryl halide radical anion and high-valent metal catalysts. In other words, a high reduction potential is required for a productive reduction by common photoredox catalysts in the presence of high valent metals, whereas a high rate constant is required for productive fragmentation. Aryl halides are generally either too difficult to reduce or fragmentation to the productive aryl radical is too slow to engage in Cu(III) metallophotoredox catalysis. Owing to their positive charge, aryldiazonium and diaryliodonium salts generally display more-positive reduction potentials than aryl halides do[3], but their synthesis is often challenging, especially at a late stage[19,20]. We measured that for any given reduction potential, ArTTs exhibit a fragmentation rate several orders of magnitude faster than that of conventional aryl halides (Supplementary Fig. 41). Combined with exquisitely selective aromatic C–H functionalization by thianthrenation[21–23], metallophotoredox catalysis can now be employed to produce synthetically valuable fluorinated analogues of complex small molecules; other one- or two-step transformations are not currently available to achieve the same goal with similar substrate scope and selectivity (Fig. 1c).

[1]Max-Planck-Institut für Kohlenforschung, Mülheim an der Ruhr, Germany. [2]Max-Planck-Institut für Chemische Energiekonversion, Mülheim an der Ruhr, Germany. [3]Global Chemistry, UCB Biopharma SPRL, Braine-l'Alleud, Belgium. *e-mail: ritter@kofo.mpg.de

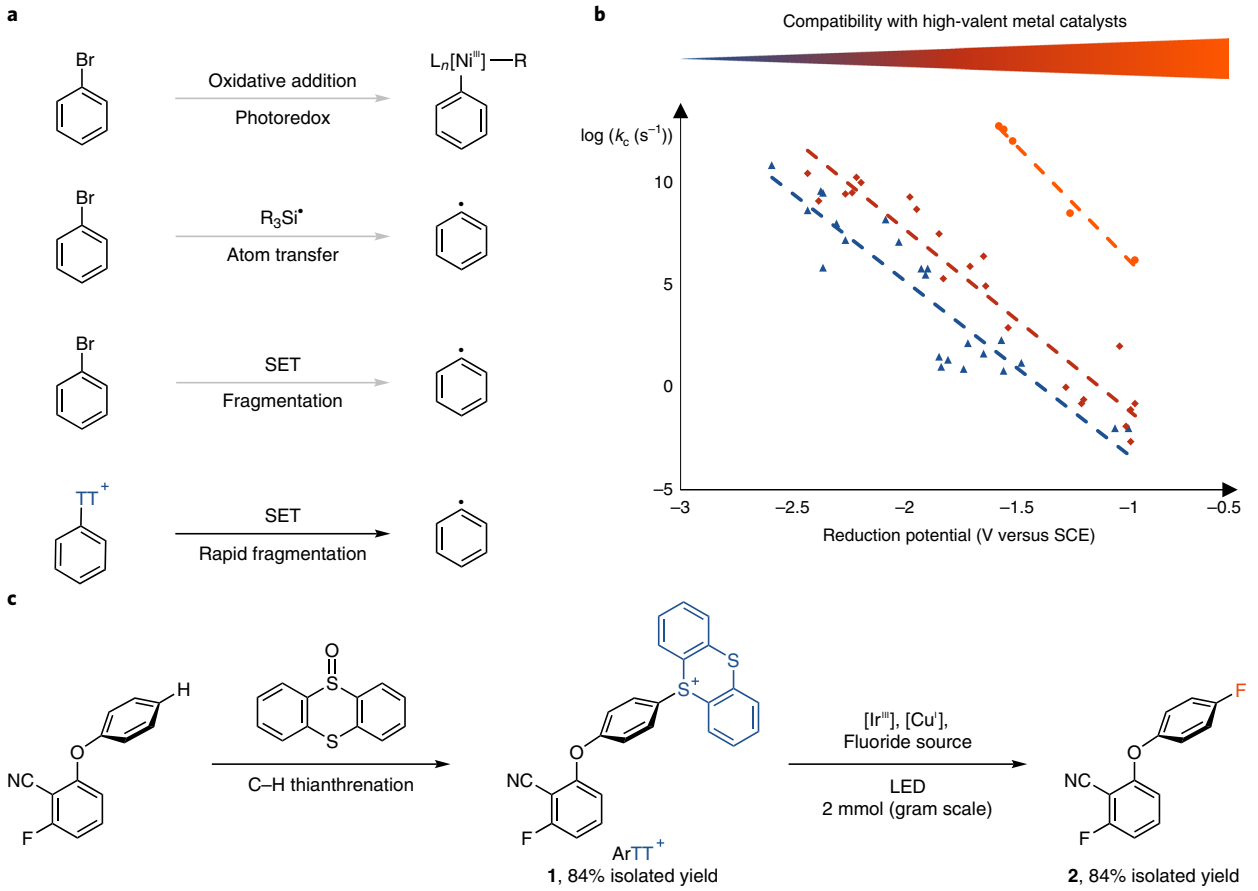

Fig. 1 | Metallophotoredox-catalysis-enabled functionalization of arenes. a, Approaches to synthetically desirable open-shell intermediates useful in photoredox catalysis. SET, single-electron transfer. **b**, Free-energy relationship between the standard reduction potential and log(rate constant k_c (s^{-1})) of mesolytic cleavage of the radical anions of aryl halides (V versus SCE in *N*,*N*-dimethylformamide) and ArTT salts (V versus SCE in CH_3CN). **c**, Specific example of C–H fluorination via an ArTT salt by metallophotoredox catalysis.

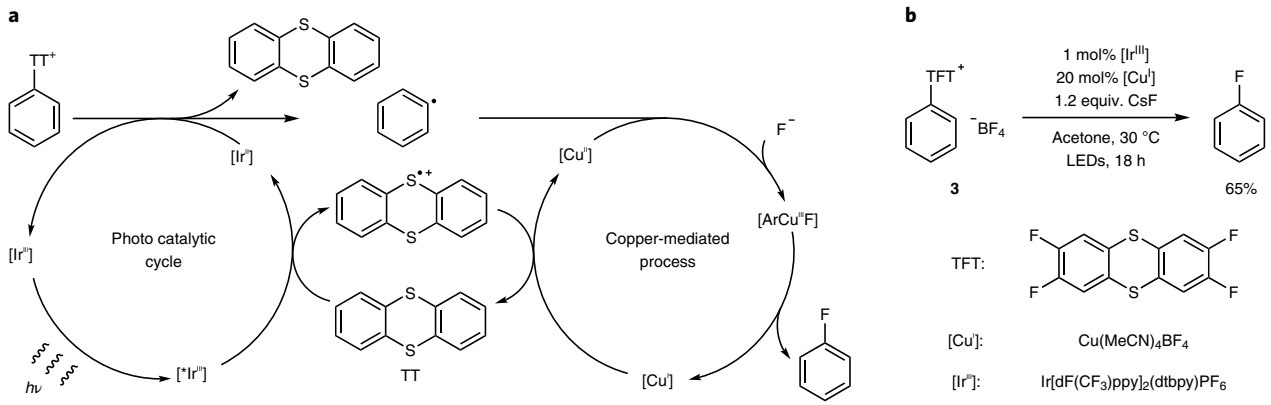

Fig. 2 | Mechanism. a, Proposed mechanism for the fluorination of $ArTT^+$ salts. **b**, Fluorination of analogous aryl tetrafluorothianthrenium ($ArTFT^+$) salt.

Results and discussion

The proposed catalytic cycle shown in Fig. 2 for a prototypical fluorination reaction with fluoride catalysed by an iridium(III) photoredox and a copper(I) redox catalyst is supported by experiments that are summarized in Fig. 3. We paid particular attention to study the fundamental differences of ArTT salts as electrophiles compared to those of more conventional electrophiles, such as aryl bromides, and to elucidate the reasons for their success in metallophotoredox catalysis. A Stern–Volmer analysis revealed an effective reductive quenching of the photoexcited iridium catalyst ($E^{0'}$ ($*Ir^{III}/Ir^{II}$) = +1.21 V versus the saturated calomel electrode (SCE) in CH_3CN)[24] by thianthrene (TT) (E^0 ($TT^{•+}/TT$) = +1.26 V versus SCE in CH_3CN][25] (Fig. 3a). Electron paramagnetic resonance (EPR) spectroscopy of the frozen reaction mixture led to the observation of both a TT radical cation and a copper(II) species during the reaction (Fig. 3b and Supplementary Figs. 17–20), consistent with the proposed mechanism and excluding the possibility of oxidative quenching of the excited iridium catalysts ($E^{0'}$ ($Ir^{IV}/*Ir^{III}$) = −0.89 V

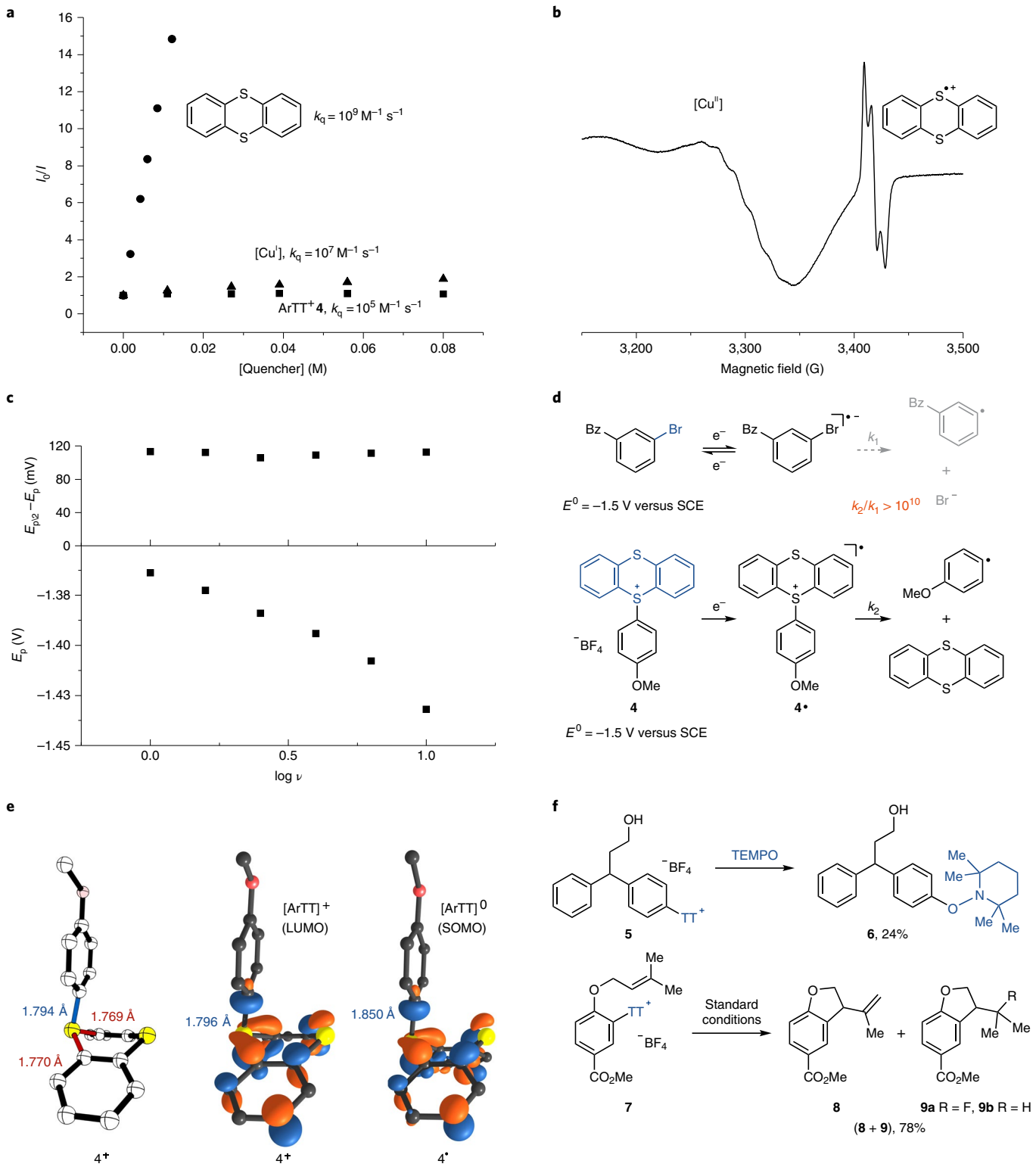

Fig. 3 | Mechanism experiments. a, Stern–Volmer plot of photocatalyst luminescence quenching by **4** (filled squares), Cu(I) (filled diamonds) and TT (filled circles). I_0, luminescence intensity without quencher; I, luminescence intensity with quencher; k_q, quenching rate constant. **b**, EPR spectrum of frozen reaction mixture. **c**, Plots of peak width and peak potential versus log υ for **4**. $E_{p/2}$, half-width potential (V versus SCE); E_p, peak potential (V versus SCE); υ, potential sweep rate (V s^{-1}). **d**, Comparative rate constants for mesolytic cleavage at similar reduction potentials. **e**, X-ray structure of [ArTT]$^+$(**4**$^+$) with relevant bond lengths (left), LUMO of [ArTT]$^+$(**4**$^+$) calculated by density functional theory (middle) and SOMO of [ArTT]^0(**4**$^•$) by density functional theory (right); *iso*-surface value = 0.06. **f**, Radical trapping experiment (top) and cyclization of prenyl ether **7** under standard reaction conditions (bottom).

versus SCE in CH_3CN)[24] by the ArTT species (E^0 (ArTT$^+$/ArTT$^•$) ≅ –1.5 V versus SCE in CH_3CN) (Supplementary Table 18). Interpretation of the hyperfine splitting of the copper-based EPR signal indicated acetonitrile ligands on Cu(II); copper fluorine bonds could not be identified by EPR, a consequence of the formation of the common copper(II) fluoride-bridged dimers which

exhibit strong antiferromagnetic coupling, and are thus not detectable by EPR spectroscopy[26].

Appropriate rates for both the reduction and subsequent fragmentation of the ArTT salts by reductive C–S bond cleavage are supported by electrochemical analyses (Fig. 3c,d). We observed an irreversible cathodic wave that corresponds to the reductive fragmentation of the 4-methoxyphenyl thianthrenium salt **4** by cyclic voltammetry between −1.2 V and −1.5 V versus SCE. Although the peak width ($E_{p/2} - E_p$) remains constant at 110 mV (Fig. 3c top), the peak potential (E_p) decreases linearly as a function of sweep rate with a slope of −65 mV, both consistent with the reductive fragmentation proceeding through a stepwise mechanism with a rate-determining initial electron transfer[27]. Although rate-determining electron transfer is only confined to the electrochemical experiments, the fragmentation rate constants are relevant to the catalytic cycle as well because they are not dependent on the rate of reduction (Supplementary pages 116–126). A Hammett analysis (Supplementary Fig. 21) is also consistent with a rate-limiting electron transfer in the photocatalytic fluorination reaction.

Owing in part to the positive charge, ArTTs are easier to reduce than aryl halides with identical substituents (Supplementary Tables 18–21). The standard reduction potential of the 4-methoxyphenyl thianthrenium salt **4** is −1.5 V versus SCE (Supplementary Table 15) and thereby similar to that of 3-bromobenzophenone[18] (Supplementary Table 19). However, the rate constant for subsequent fragmentation of both corresponding reduced species is at least ten orders of magnitude faster for the TT radical species, which cannot be explained by the reduction potential (Fig. 3d). Although complex leaving groups other than TT, for example, as found in diarylalkyl sulfonium salts, might have appropriate redox potentials for facile reduction, undesired side reactions on single-electron reduction may render them synthetically useless. For example, diarylalkyl sulfonium salts are strong alkylating reagents and reduction by single-electron transfer leads to unselective fragmentation to afford aryl and alkyl radicals[28], which renders them unsuitable for analogous metallophotoredox catalysis. ArTT salts have three C–S bonds, but synthetic utility can only be harnessed if chemoselective cleavage of the exocyclic C–S bond is achieved in preference to that of the other two endocyclic C–S bonds. X-ray crystallographic analysis of a variety of ArTT salts (Fig. 3e and Supplementary Figs. 42–46) shows the aryl substituent in a flagpole position with respect to the dithiine, with a significantly longer C–S bond than the other two C–S bond lengths within the TT scaffold. Its chemoselective mesolytic cleavage can also be rationalized as a consequence of the antibonding nature of the exocyclic aryl C–S bond in the lowest unoccupied molecular orbital (LUMO) of $[ArTT]^+$(**4**) and its lengthening on reduction to the $[ArTT]^0$ radical (**4**$^\cdot$), as calculated by density functional theory (Fig. 3e and Supplementary Table 30). The larger rate of ArTT radical fragmentation when compared to that of aryl bromide radical anion fragmentation can thus be explained by the stereoelectronic alignment of the σ^* orbital of the exocyclic C–S bond with the π system of the TT scaffold (Supplementary Fig. 48). The mesolytic cleavage of aryl bromides requires a bending motion to achieve sufficient population of the C–Br σ^* orbital, which is orthogonal to the π framework; in both cases, the singly occupied molecular orbital (SOMO) has the largest parentage in the π framework, but only in the ArTTs is it appropriately aligned to expel the leaving group[29–31]. The TT-based LUMO of the ArTT salts can also explain why their reduction potentials are less sensitive to substituent effects on the arene, which can be extracted from the length of the respective lines in Fig. 1b and quantified (Supplementary Fig. 49).

Consistent with the formation of aryl radicals during catalysis, the 2,2,6,6-tetramethylpiperidin-1-oxyl (TEMPO) adduct could be isolated under the reaction conditions on addition of TEMPO. Likewise, the same adduct (**6**) was also observed when copper(I) was excluded from the reaction mixture, which rules out the possibility of a copper-mediated C–O coupling between $[ArTT]^+$**3** and TEMPO. Furthermore, observation of cyclization products in a 78% combined yield of the prenyl ether **7** under standard reaction conditions supports a mechanism that proceeds through aryl radicals. Our analysis is consistent with the observation that the optimized reaction conditions of copper-mediated photoredox catalysis can also elicit fluorination from aryldiazonium salts, which have higher reduction potentials than the corresponding halides: phenyldiazonium tetrafluoroborate was converted into fluorobenzene in 37% yield upon photolysis in the presence of an iridium catalyst and copper(I) salt (Supplementary Fig. 3).

Owing to their desirable properties, most notably in pharmaceuticals and agrochemicals, aryl fluorides are highly sought after. Several electrophilic fluorination reactions from aryl nucleophiles, such as aryl boronates, are available[32–34], but such aryl nucleophiles are often not readily available selectively or at all from complex small molecules. Palladium-catalysed nucleophilic fluorination has been developed successfully, yet protic functional groups and other groups that engage in palladium-catalysed cross-coupling, such as other halides, may pose problems[35]; in addition, aryl electrophile starting materials, such as aryl halides, are generally not accessible selectively at a late stage[21]. Only one direct, late-stage C–H fluorination reaction of arenes is available, but the product mixtures that result must be separated from other constitutional isomers and unreacted starting material, which can be challenging[36]. The two-step late-stage fluorination reaction we present here selectively produces a single constitutional isomer, enables trivial purification from the ionic starting material, is tolerant of a wide variety of functional groups, which include several that are not tolerated in palladium-catalysed cross-coupling and electrophilic fluorination reactions, and can therefore quickly give access to complex small molecule aryl fluorides that are not readily accessible by current methods.

As shown in Fig. 2b, copper catalysis is possible for fluorination. Yet, purification of aryl fluorides from the corresponding hydro-counterparts is challenging. The addition of a stoichiometric amount of inexpensive Cu(I) salt eliminated the undesired amounts of hydrodefunctionalized side product of complex small molecules that could be observed for reactions with catalytic copper. All the non-volatile fluorides shown in Table 1 could therefore be isolated as analytically pure compounds. The use of acetone as the solvent also had a major effect on the suppression of the hydrodefunctionalization reaction. Typically, the reaction was performed at 0.1 M concentration, although higher concentrations (0.5 M) did not result in a lower yield in the evaluated cases (Supplementary Table 8). Both ArTT and tetrafluorothianthrenium salts can successfully participate in fluorination, and the thianthrenium congeners typically afforded higher yield (Supplementary Table 2). Fluorination is successful on electron-deficient (**10**, **11** and **15**), -neutral (**18**, **25** and **26**) and -rich arenes (**13**, **31** and **38**), as well as on substrates that bear *ortho* substituents (**12**, **20**, **21**, **24**, **28**, **30** and **34**). The reaction is tolerant towards aldehydes (**17**), esters (**16** and **19**), heterocycles (**23**, **24**, **29** and **39**), benzyl ethers (**31**), carbamates (**36**), amides (**22**, **32**, **33** and **37**), acid-sensitive glycosidic linkages (**14**) and enolizable groups, such as ketones (**28**). Protic groups, such as alcohols (**26**) and phenols (**20**), all the halides (**10**–**12**, **15**, **19**, **24**, **27**, **29**, **32** and **33**), pseudo-halides (**35**) and tertiary amines (**29**), many of which are not compatible with other nucleophilic and electrophilic transition metal-catalysed fluorination reactions, are tolerated in copper-mediated photoredox fluorination.

Conclusions

Aryl fluorides are now available at the late-stage in high, predictable selectivity through a thianthrenation followed by metallophotoredox–catalysis reaction sequence. We articulate the specific electrochemical, structural and stereoelectronic requirements for

Table 1 | Substrate scope of the fluorination of thianthrenium salts under photoredox conditions

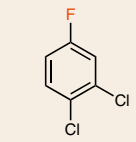

10 (20%)[c], 63%[d]

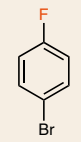

11 (74%), 72%[d]

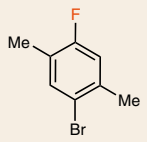

12 (41%), 67%

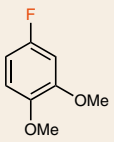

13 (76%)[c], 75%

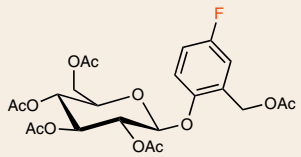

14 (93%), 77%
F-salicin pentaacetate

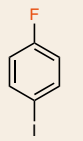

15 (74%), 71%[d]

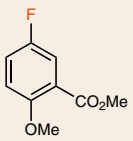

16 (78%), 79%

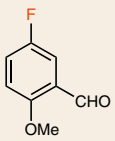

17 (83%), 68%

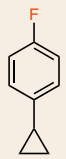

18 (92%), 71%

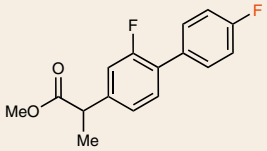

19 (67%), 78%
F-flurbiprofen methyl ester

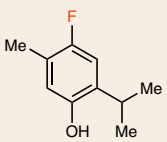

20 (79%), 41%

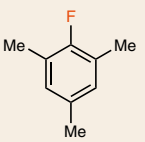

21 (62%), 42%[d]

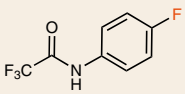

22 (73%), 81%

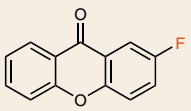

23 (78%), 70%

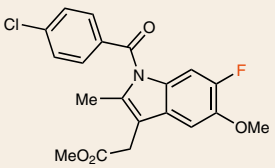

24 (85%)[c], 33%
F-indomethacin methylester

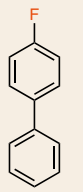

25 (81%), 73%

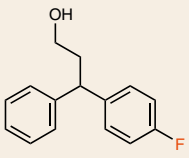

26 (28%), 78%

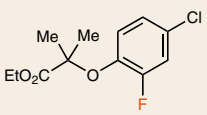

27 (88%), 60%
F-clofibrate ethyl ester

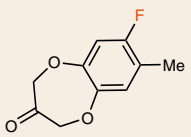

28 (79%), 69%
F-calone

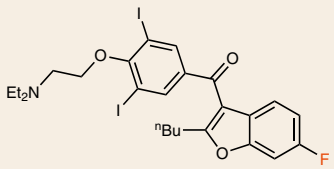

29 (92%)[c], 35%
F-amiodarone

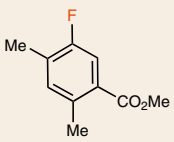

30 (93%), 84%

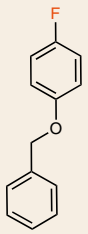

31 (58%), 76%

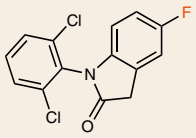

32 (46%), 58%
F-diclofenac derivative

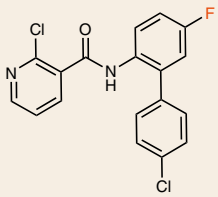

33 (95%)[c], 62%
F-boscalid

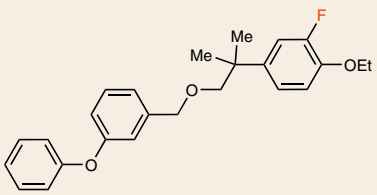

34 (84%)[c], 80%
F-etofenprox

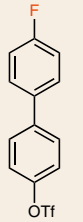

35 (66%)[c], 82%

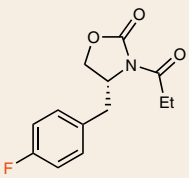

36 (87%)[c], 80%

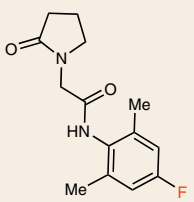

37 (63%)[c], 42%
F-nefiracetam

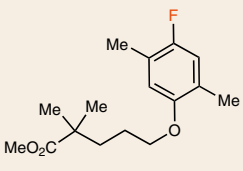

38 (79%), 81%
F-gemfibrozil methyl ester

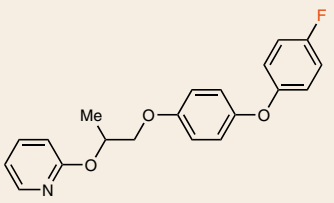

39 (92%)[c], 52%
F-pyriproxyfen

Reaction conditions: (tetrafluoro)thianthrenium salt (0.20 mmol, 1.0 equiv.), CsF (1.2 equiv.), $[Cu(MeCN)_4]BF_4$ (1.5 equiv.), $[Ir[dF(CF_3)ppy]_2(dtbpy)PF_6]$ (1 mol%), acetone (0.1 or 0.2 M), blue light-emitting diode (68 W), 30 °C, 20 h. All non-volatile fluorinated products were isolated and characterized as analytically pure samples. [a]Yield of thianthrenation. [b]Yield of fluorination. [c]Yield of the thianthrenation from Berger et al.[21]. [d]Yields of volatile fluorides are reported based on the ^{19}F NMR integration of reaction mixtures with internal standard.

aryl leaving groups to address the challenge of copper(III)-mediated photoredox catalysis as a promising reactivity manifold. In contrast to mononuclear leaving groups, such as bromide, complex leaving groups can bear a positive charge that can lower the reduction potential while they maintain the ability to engage in productive redox catalysis if they display appropriate stereoelectronic properties. Therefore, the conceptual value of our contribution is also to provide a suitable hypothesis for the design of new leaving groups that do not undergo deleterious side reactions and so can also engage in metallophotoredox catalysis with copper or other metals.

Methods

General procedure for fluorination. To a 4 ml borosilicate vial, equipped with a stir bar, was added $Ir[dF(CF_3)ppy]_2(dtbpy)PF_6$ (2.4 mg, 2.1 µmol, 1.0 mol%) ($dF(CF_3)ppy$, 2-(2,4-difluorophenyl)-5-(trifluoromethyl)pyridine; dtbbpy, 4,4′-di-*tert*-butyl-2,2′-bipyridine)) and an aryl (tetrafluoro)thianthrenium salt (0.200 mmol, 1.00 equiv.). Under N_2 atmosphere, $Cu(MeCN)_4BF_4$ (94.4 mg, 0.300 mmol, 1.50 equiv.), anhydrous CsF (36.4 mg, 0.240 mmol, 1.20 equiv.) and anhydrous acetone (2.0 ml, 0.10 M) were added into the reaction vial. Subsequently, the vial was capped and placed 5 cm away from two 34 W blue light-emitting diode (LEDs). The temperature was kept at approximately 30 °C through cooling with a fan. After being stirred for 20 h, the reaction mixture was diluted with CH_2Cl_2 (2 ml) and the resulting mixture was filtered through a short pad of Celite using CH_2Cl_2 (5 ml) as eluent. The filtrate was collected and concentrated by rotary evaporation. The residue was purified by chromatography on silica gel to afford the fluorinated product.

Note that for the optimal results, the use of anhydrous CsF is important for the reaction. When CsF was weighed under ambient atmosphere, the yield of the fluorinated product was lower and the yield of the hydrodefunctionalized product was higher. Schlenk techniques can be used to avoid moisture. For convenience, we stored and weighed the CsF in a N_2-filled glove box; the reactions can be performed outside a glove box.

Data availability

Crystallographic data for the structures reported in this article have been deposited at the Cambridge Crystallographic Data Centre (CCDC) under deposition numbers CCDC 1900278 (**4**), 1900279 (**25-TT**), 1900280 (**40-TT**), 1900276 (**41-TT**) and 1900277 (**43-TT**) (Supplementary Figs. 42–46). Copies of the data can be obtained free of charge via https://www.ccdc.cam.ac.uk/structures/. All other data that support the findings of this study are available within the article and its Supplementary Information, or from the corresponding author upon reasonable request.

Received: 24 April 2019; Accepted: 17 September 2019;
Published online: 25 November 2019

References

1. Twilton, J. et al. The merger of transition metal and photocatalysis. *Nat. Rev. Chem.* **1**, 0052 (2017).
2. Tellis, J. C. et al. Single-electron transmetalation via photoredox/nickel dual catalysis: unlocking a new paradigm for sp^3–sp^2 cross-coupling. *Acc. Chem. Res.* **49**, 1429–1439 (2016).
3. Ghosh, I., Marzo, L., Das, A., Shaikh, R. & König, B. Visible light mediated photoredox catalytic arylation reactions. *Acc. Chem. Res.* **49**, 1566–1577 (2016).
4. Skubi, K. L., Blum, T. R. & Yoon, T. P. Dual catalysis strategies in photochemical synthesis. *Chem. Rev.* **116**, 10035–10074 (2016).
5. Zuo, Z. et al. Merging photoredox with nickel catalysis: coupling of α-carboxyl sp^3-carbons with aryl halides. *Science* **345**, 437–440 (2014).
6. Tellis, J. C., Primer, D. N. & Molander, G. A. Single-electron transmetalation in organoboron cross-coupling by photoredox/nickel dual catalysis. *Science* **345**, 433–436 (2014).
7. Stache, E. E., Rovis, T. & Doyle, A. G. Dual nickel- and photoredox-catalyzed enantioselective desymmetrization of cyclic meso-anhydrides. *Angew. Chem. Int. Ed.* **56**, 3679–3683 (2017).
8. Corcoran, E. B. et al. Aryl amination using ligand-free Ni(II) salts and photoredox catalysis. *Science* **353**, 279–283 (2016).
9. Terrett, J. A., Cuthbertson, J. D., Shurtleff, V. W. & MacMillan, D. W. C. Switching on elusive organometallic mechanisms with photoredox catalysis. *Nature* **524**, 330–334 (2015).
10. Welin, E. R., Le, C., Arias-Rotondo, D. M., McCusker, J. K. & MacMillan, D. W. C. Photosensitized, energy transfer-mediated organometallic catalysis through electronically excited nickel(II). *Science* **355**, 380–385 (2017).
11. Lee, E., Hooker, J. M. & Ritter, T. Nickel-mediated oxidative fluorination for PET with aqueous [^{18}F] fluoride. *J. Am. Chem. Soc.* **134**, 17456–17458 (2012).
12. Ribas, X. & Casitas, A. in *Ideas in Chemistry and Molecular Sciences: Where Chemistry Meets Life* (ed. B. Pignataro) 31–57 (Wiley-VCH, 2010).
13. Casitas, A., Canta, M., Solà, M., Costas, M. & Ribas, X. Nucleophilic aryl fluorination and aryl halide exchange mediated by a Cu^{I}/Cu^{III} catalytic cycle. *J. Am. Chem. Soc.* **133**, 19386–19392 (2011).
14. Le, C., Chen, T. Q., Liang, T., Zhang, P. & MacMillan, D. W. C. A radical approach to the copper oxidative addition problem: trifluoromethylation of bromoarenes. *Science* **360**, 1010–1014 (2018).
15. Ghosh, I., Ghosh, T., Bardagi, J. & König, B. Reduction of aryl halides by consecutive visible light-induced electron transfer processes. *Science* **346**, 725–728 (2014).
16. Ghosh, I. & König, B. Chromoselective photocatalysis: controlled bond activation through light-color regulation of redox potentials. *Angew. Chem. Int. Ed.* **55**, 7676–7679 (2016).
17. Nguyen, J. D., D'Amato, E. M., Narayanam, J. M. R. & Stephenson, C. R. J. Engaging unactivated alkyl, alkenyl and aryl iodides in visible-light-mediated free radical reactions. *Nat. Chem.* **4**, 854–859 (2012).
18. Costentin, C., Robert, M. & Savéant, J. M. Fragmentation of aryl halide π anion radicals. Bending of the cleaving bond and activation vs driving force relationships. *J. Am. Chem. Soc* **126**, 16051–16057 (2004).
19. Yang, S., Chen, M. & Tang, P. Visible-light photoredox-catalyzed and copper-promoted trifluoromethoxylation of arenediazonium tetrafluoroborates. *Angew. Chem. Int. Ed.* **58**, 7840–7844 (2019).
20. Ichiishi, N., Canty, A. J., Yates, B. F. & Sanford, M. S. Cu-catalyzed fluorination of diaryliodonium salts with KF. *Org. Lett.* **15**, 5134–5137 (2013).
21. Berger, F. et al. Site-selective and versatile aromatic C–H functionalization by thianthrenation. *Nature* **567**, 223–228 (2019).
22. Ye, F. et al. Aryl sulfonium salts for site-selective late-stage trifluoromethylation. *Angew. Chem. Int. Ed.* **58**, 14615–14619 (2019).
23. Engl, P. S. et al. C–N cross-couplings for site-selective late-stage diversification via aryl sulfonium salts. *J. Am. Chem. Soc.* **141**, 13346–13351 (2019).
24. Lowry, M. S. et al. Single-layer electroluminescent devices and photoinduced hydrogen production from an ionic iridium(III) complex. *Chem. Mater.* **17**, 5712–5719 (2005).
25. Hammerich, O. & Parker, V. D. The reversible oxidation of aromatic cation radicals to dications. Solvents of low nucleophilicity. *Electrochim. Acta* **18**, 537–541 (1973).
26. Rupp, H., Verplaetse, J. & Lontie, R. Binuclear copper electron paramagnetic resonance signals of α-methemocyanin of helix pomatia. *Z. Naturforsch.* **35 c**, 188–192 (1980).
27. Andrieux, C. P., Savéant, J.-M., Tallec, A., Tardivel, R. & Tardy, C. Concerted and stepwise dissociative electron transfers. Oxidability of the leaving group and strength of the breaking bond as mechanism and reactivity governing factors illustrated by the electrochemical reduction of α-substituted acetophenones. *J. Am. Chem. Soc.* **119**, 2420–2429 (1997).
28. Kampmeier, J. A. et al. Regioselectivity in the reductive bond cleavage of diarylalkylsulfonium salts: variation with driving force and structure of sulfuranyl radical intermediates. *J. Am. Chem. Soc.* **131**, 10015–10022 (2009).
29. Laage, D., Burghardt, I., Sommerfeld, T. & Hynes, J. T. On the dissociation of aromatic radical anions in solution. 1. Formulation and application to *p*-cyanochlorobenzene radical anion. *J. Phys. Chem. A* **107**, 11271–11291 (2003).
30. Burghardt, I., Laage, D. & Hynes, J. T. On the dissociation of aromatic radical anions in solution. 2. Reaction path and rate constant analysis. *J. Phys. Chem. A* **107**, 11292–11306 (2003).
31. Laage, D., Burghardt, I., Sommerfeld, T. & Hynes, J. T. On the dissociation of aromatic radical anions in solution. *ChemPhysChem* **4**, 61–66 (2003).
32. Fier, P. S., Luo, J. & Hartwig, J. F. Copper-mediated fluorination of arylboronate esters. Identification of a copper(III) fluoride complex. *J. Am. Chem. Soc.* **135**, 2552–2559 (2013).
33. Ye, Y. & Sanford, M. S. Mild copper-mediated fluorination of aryl stannanes and aryl trifluoroborates. *J. Am. Chem. Soc.* **135**, 4648–4651 (2013).
34. Ye, Y., Schimler, S. D., Hanley, P. S. & Sanford, M. S. $Cu(OTf)_2$-mediated fluorination of aryltrifluoroborates with potassium fluoride. *J. Am. Chem. Soc.* **135**, 16292–16295 (2013).
35. Watson, D. A. et al. Formation of ArF from LPdAr(F): catalytic conversion of aryl triflates to aryl fluorides. *Science* **325**, 1661–1664 (2009).
36. Yamamoto, K. et al. Palladium-catalysed electrophilic aromatic C–H fluorination. *Nature* **554**, 511–514 (2018).

Acknowledgements

We thank C. Costentin (Université Paris VII) for helpful discussions on the electrochemical analysis. We thank O. Rüdiger (MPI CEC) for providing the electrochemical set-up and for helpful discussions, S. Marcus and D. Kampen (MPI KOFO) for mass spectrometry analysis and A. Dreier and J. Rust (MPI KOFO) for the crystal structure analysis.

Author contributions

J.L., J.C. and R.S. developed the fluorination reaction. W.-S.H., M.B.P, J.L., J.C., F.B., S.C., A.S. and C.G. contributed to the mechanistic studies. F.B. initiated the approach to the project. All the authors wrote the manuscript. T.R. directed the project.

Competing interests

A patent application (German patent number EP18204755.5), dealing with the use of TT and its derivatives for C–H functionalization has been filed, and F.B. and T.R. may benefit from royalty payments.

Additional information

Supplementary information is available for this paper at https://doi.org/10.1038/s41557-019-0353-3.

Correspondence and requests for materials should be addressed to T.R.

Reprints and permissions information is available at www.nature.com/reprints.

Publisher's note Springer Nature remains neutral with regard to jurisdictional claims in published maps and institutional affiliations.